ARCHIVES OF METALLURGY
Volume 48 2003 Issue 1

JOSE C. ESCOBEDO BOCARDO*, LUZ del CARMEN PEDROZA CERVANTES*
JANUSZ DONIZAK**, ZYGMUNT KOLENDA**

NUMERICAL MODELING AND EXPERIMENTAL INVESTIGATION OF Co-Cr-Mo ALLOYS SOLIDIFICATION

MODELOWANIE NUMERYCZNE I BADANIA EKSPERYMENTALNE KRZEPNIĘCIA STOPÓW Co-Cr-Mo

Solidification modeling based on classical macroscopic energy, mass, momentum and solute continuity equations does not allow to predict of microstructural parameters satisfactorily. In past decades several attemps have been made for the developing of modelling methodology for the coupling macro transport equations with the transformation kinetics in the micro scale. The micromodeling focused to the multicomponent alloys is still rare, despite the majority of the new industrial alloys are formed from complex multicomponent systems. The paper presents the micromodeling procedure coupled with thermodynamic calculation and experimental investigations for the Co-Cr-Mo alloys, frequently used as biomaterials for the production of endoprotheses. Both, experimental and numerical results showed that: the grain structure is mainly influenced by the cooling rate, the partition coefficients exhibit significant dependency on the cooling rate (especially for molybdenum), the high cooling rate promotes early formation of fine intragranular carbides. The experimentally obtained values of latent heat of solidification exhibit important dependency on the initial carbon content, and cannot be ignored in solidification simulations. The solidification modeling results have been verified using cooling curve analysis and metallografic investigations. It seems, that the model can be used in engineering applications for solidification simulations.

Modelowanie krzepnięcia stopów metali oparte na klasycznych makroskopowych równaniach bilansu pędu, energii, masy nie pozwalają na symulacje mikrostrukturalnych parametrów odlewów z wystarczającą precyzją. W ostatnich dekadach podjęto szereg prób w celu opracowania metodologii modelowania matematycznego procesu krzepnięcia, które bazują na sprzęgnięciu makroskopowych równań transportu z kinetyką transformacji fazowej w skali mikroskopowej. Jednak prace poświęcone modelowaniu krzepnięcia stopów wieloskładnikowych są nadal rzadkie, mimo iż stopy te mają istotne znaczenie przemysłowe. Artykuł przedstawia propozycję procedury

* CINVESTAV UNIDAD SALTILLO, CARRETERA SALTILLO–MONTERREY KM 13.5, A.P. 663, SALTILLO, COAHUILA, MEXICO
** KATEDRA TEORII I INŻYNIERII PROCESÓW METALURGICZNYCH, WYDZIAŁ METALI NIEŻELAZNYCH, AGH, 30-059 KRAKÓW, AL. MICKIEWICZA 30

obliczeniowej mikromodelu skojarzonej z obliczeniami termodynamicznymi i badaniami eksperymentalnymi dla stopów na bazie układu Co-Cr-Mo, które znajdują zastosowanie przy produkcji bio-materiałów do wytwarzania endoprotez. Zarówno wyniki eksperymentalne jak i rozwiązania modelowe potwierdzają, iż struktura ziarnowa badanych stopów oraz współczynniki podziału (zwłaszcza w odniesieniu do molibdenu) wykazują istotną zależność od szybkości studzenia, oraz iż wysoka szybkość studzenia promuje wczesne tworzenie się wewnątrzziarnowych węglików. Ponadto, eksperymentalnie wyznaczone utajone ciepło krzepnięcia wykazuje istotną zależność od zawartości węgla, co winno być uwzględnione w procedurach symulacji krzepnięcia. Wyniki obliczeń numerycznych weryfikowano przez analizę krzywej studzenia stopu i badania metalograficzne. Opracowany model powiązany ze standardowym oprogramowaniem transportu pędu, masy i ciepła może być wykorzystywany do symulacji krzepnięcia stopów kobaltowych w zastosowaniach inżynieryjnych.

List of symbols

A_1, A_2, A_3 – coefficients, Eq. (33),
c_p – volumic specific heat,
D – solute diffusion coefficient in the liquid,
D_i – diffusion coefficient for constituent i in the liquid,
E – average temperature gradient near the dendrite tip,
E_{xi} – solute gradient of constituent i near the dendrite tip,
$F(\ )$ – general function,
f_S – volume solid fraction,
f_g – grain volume fraction of the freely growing equiaxed dendritic grains,
f_i – internal solid volume fraction (with respect to the growing grain volume),
${}^{ex}G$ – excess free energy for real solutions (non-ideal mixing),
${}^{ex}G_i$ – partial excess free energy of component i,
${}^{ex}G_{ij}$ – excess free energy of binary system i-j,
${}^{o}G_{F,i}$ – partial free energy of ideal mixing at standard state of component i in phase F,
${}^{ex}G_{F,i}$ – excess partial free energy for component i in phase F,
H – volumic enthalpy,
ΔH^{m+1} – volumic enthalpy extracted from the control volume element at time step $m+1$ of macro transport equation solution procedure,
Δh – volumic enthalpy extracted from the control volume element at time step of micro-model solution procedure,
k – partition coefficient,
k_i – partition coefficient for constituent i,
L – volumic latent heat of fusion,
M – number of micro-model time steps $\Delta\tau$ per one macro-model time step Δt,
m_i – slope of the liquidus line in the corresponding binary system (base component vs i component),
N – number of constituents in the multicomponent system,
n – number of active nuclei,
$n_{\max}$ – maximum density of nuclei attainable at the infinite undercooling ΔT,
Pe – grain Peclet number, $Pe = vR/2D$,
Pe_i – Peclet number associated with the moving tip of the dendrite paraboloid for constituent i, $Pe_i = r_p v/2D_i$,
Q – cooling rate of the sample during experiment,
R – radius of the equiaxed dendritic grain, determined by the location of dendrite tips,
r_p – radius of dendrite tip,

T – temperature,
t – time,
T_L – liquidus temperature for the initial alloy composition x_0,
ΔT – undercooling,
ΔT_n – mean value of nucleation undercooling (parameter of the distribution function),
ΔT_σ – standard deviation of the nuclei distribution (parameter of the distribution function),
Δt^{m+1} – time step length of macro transport equation solution procedure,
$\Delta \tau$ – micro time step length in micro-model solution procedure,
V – volume,
x – concentration,
X_i^{ij} – mole fraction of component i in the binary system ij,
$x_{L,i}$ – liquid concentration of component i,
$x_{S,i}$ – solid concentration of component i,
x_L^* – liquid concentration of the solute at the dendrite tip,
x_S^* – solid concentration of solute in equilibrium with liquid of composition x^*_L,
x_O – liquid concentration of solute in the bulk liquid (initial concentration).

Greek symbols
Γ – Gibbs-Thomson coefficient of the alloy,
$\Re$ – universal ideal gas constant,
μ – chemical potential,
$\mu_{F,i}$ – chemical potential of component i in phase F,
Ω – supersaturation, $\Omega = \dfrac{x^*_L - x_O}{x^*_L - x^*_S}$,
ν – velocity of the dendrite tip,
β – coefficient, Eq. (15),
η – kinetic constant, Eq. (23),
$\psi(\ )$ – impingement weighting function, Eq. (25),
$\phi(\ )$ – function defined in Eq. (13),
ε – fraction of solute mixed into the bulk liquid,
$\zeta_x(Pe)$ – stability parameter, Eq. (31).

Super- and subscripts
0 – initial value,
F – phase index,
g – grain,
i – component index in multicomponent system,
k – index of micro-model time step,
L – liquid phase,
m – index of macro-model time step,
S – solid phase.

1. Introduction

The metal alloys solidification process plays the most important role in the determining the properties of the foundry products. The solidification structures of castings influence the mechanical properties and corrosion resistance of the product. Cobalt based alloys, frequently used as biomaterials for the production of endoprotheses, must exhibit high

corrosion resistance in the physiological solutions and proper mechanical strenght (endurance) [1]. The control of the grain structure and solute microsegregation is of primary importance in solidyfying processes, which can be accesed by means of controling heat flow conditions and alloy composition. Solidification modeling based on classical macroscopic energy, mass, momentum and solute continuity equations does not allow to predict of microstructural parameters satisfactorily. In past decades several attemps have been made for the developing of modelling methodology for the coupling macro transport equations with the transformation kinetics in the micro scale [2]. The micromodeling focused to the multicomponent alloys is still rare, despite the majority of the new industrial alloys are formed from complex multicomponent systems. It has been found that the alloying elements, even in low concentrations, significantly influence microstructure and microsegregation [3]. The assumption of constant partition coefficient and linearisation procedure of equilibrium phase diagram used for binary alloys is unacceptable for multicomponent ones. In the paper, we try to exploit several modeling techniques for development of adequate deterministic solidification micro-model, which can be used in standard micro/macro enthalpy computer code for simulation industrial castings. Model predictions are compared with experimental results obtained for multicomponent cobalt based alloy (ASTM F-75) solidification process.

2. Thermodynamics of multicomponent system

The starting point for any alloy solidification problem is the equilibrium phase diagram for the system in question. In order to predict the paths of solidification of a multi-component alloy (such as ASTM F-75) it is essential to know its liquid-solid phase equilibrium diagram. The lack of experimental equilibrium data of such complex multi-component system enforced us to model the equilibrium system on the basis of thermodynamic considerations. The heterogeneous equilibrium condition of n-component system is expressed by the set of equations [4, 5]:

$$\mu_{L,i} = \mu_{S,i} \qquad i = 1,..,N \tag{1}$$

expressing the equality of a chemical potential μ of each component in two phases

$$\mu_{F,i} = {}^{\circ}G_{F,i} + \Re T \ln x_{F,i} + {}^{ex}G_{F,i}, \tag{2}$$

where F stands for L (liquid phase) or S (solid phase).

Following the generalized conception of Chou and Chang [6] the derivation of Gibbs energies of 3 component system from those of three binary system, the excess free energy of ternary system i-j-k can be evaluated from:

$${}^{ex}G = \sum w_{ij}\, {}^{ex}G_{ij} \qquad (ij = 12,\ 13,\ 23), \tag{3}$$

where excess free energy ${}^{ex}G_{ij}$ of binary system i-j, expressed as

$$ {}^{ex}G_{ij} = X_i^{ij} X_j^{ij} [A_{ij} + B_{ij}(X_i^{ij} - X_j^{ij}) + C_{ij}(X_i^{ij} - X_j^{ij})^2]. \quad (4) $$

The parameters A_{ij}, B_{ij}, C_{ij} of the binary system model are in general functions of temperature, and must obey the following constraints

$$ A_{ii} = B_{ii} = C_{ii} = 0, \; A_{ij} = A_{ji}, \; B_{ij} = -B_{ji}, \; C_{ij} = C_{ji} $$

and the weighting factors are defined as

$$ w_{ij} = (x_i x_j) / (X_i^{ij} X_j^{ij}). \quad (5) $$

The generalization of eq. (3) leads to the N component systems of the form:

$$ {}^{ex}G = \sum_{i=1}^{N-1} \sum_{j=i+1}^{N} x_i x_j [A_{ij} + B_{ij} (X_i^{ij} - X_j^{ij}) + C_{ij} (X_i^{ij} - X_j^{ij})^2]. \quad (6) $$

Several geometrical models, relating x_i and x_j with $X_i^{ij} X_j^{ij}$ have been proposed up to date. In present calculation we have used simple Colinet model [5], where $X_i^{ij} = x_i$, $X_j^{ij} = x_j$, $X_i^{ij} - X_j^{ij} = 2x_i - 1$.

For the ternary system, the excess free Gibbs energies ${}^{ex}G_1$, ${}^{ex}G_2$, ${}^{ex}G_3$ are given by:

$$ \begin{aligned} {}^{ex}G_1 &= {}^{ex}G - x_2 \, (\partial {}^{ex}G_2 / \partial x_2) - x_3 \, (\partial {}^{ex}G_3 / \partial x_3) \\ {}^{ex}G_2 &= {}^{ex}G_1 + (\partial {}^{ex}G_2 / \partial x_2) \\ {}^{ex}G_3 &= {}^{ex}G_1 + (\partial {}^{ex}G_3 / \partial x_3). \end{aligned} \quad (7) $$

Finally, the system of equations defining the equilibrium between liquid and solid phase in ternary system takes the form

$$ ({}^{\circ}G_{L,i} - {}^{\circ}G_{S,i}) + (\Re T \ln x_{L,i} - \Re T \ln x_{S,i}) + ({}^{ex}G_{L,i} - {}^{ex}G_{S,i}) = 0; \quad i = 1, 2, 3 \quad (8) $$

with 7 variables (3 molar fractions of liquid, 3 molar fractions of solid, and temperature). Knowing the composition of other phase, and having in mind that only 2 of molar fractions of solid are independent variables, due to the solid phase mass balance equation

$$ x_{S,1} + x_{S,2} + x_{S,3} = 1 \quad (9) $$

the equation set (8) can be used to obtain unique temperature (liquidus temperature) and solid composition in equilibrium with liquid phase. Because the system of equations (8) is

nonlinear, its solution is not straightforward, and an efficient numerical technique has to be used to solve it.

TABLE 1

Thermodynamic parameters for solid and liquid phases (eq. (4))

Binary system i-j	A_{ij}(T) [J]	B_{ij}(T) [J]	C_{ij}(T) [J]	reference
Liquid phase				
Cr-Co	−29429.0	0.0	0.0	[5], [7]*
Cr-Mo	19037.0−8.58 · T	6485.0−2.72 · T	0.0	[5]
Co-Mo	2510.0	0.0	0.0	[5]
Solid phase				
Cr-Co	−47554.0	0.0	0.0	[5], [7]*
Cr-Mo	27823.5−8.58 · T	6485.0−2.72 · T	0.0	[5]
Co-Mo	−25104.0+20.92 · T	0.0	0.0	[5]

* Orginal data verified against thermodynamic data from [7]

Equilibrium diagram (solid — liquid region) for the ASTM F75 alloy used in our work has been prepared neglecting minor alloying elements (such as Mn, Si, Ni, Fe, W and C), however incorporation of these elements can be easily done. Therefore, we have reduced a number of components to three. Thermodynamic data used in computations are those reported in [5] and given in Table 1.

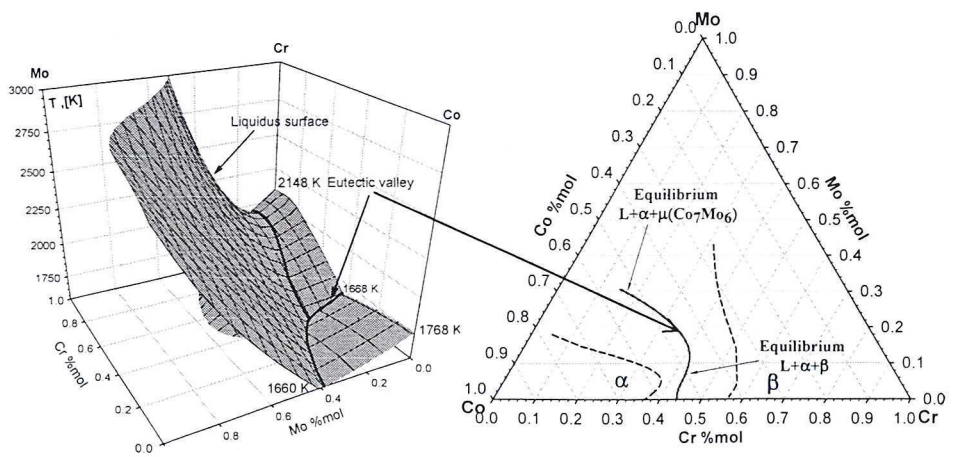

Fig. 1. Liquidus surface projection of Co-Cr-Mo ternary system based on thermodynamic data

The calculated liquidus projection of the ternary Co-Cr-Mo system is shown in Fig. 1. It shows, that the Co-Cr-Mo system forms the eutectic valleys. The equilibrium system of equations (8) can be used not only for the preparation of the equilibrium diagram, but also for solidification modeling purposes, as shown in next part of the paper. Moreover, the values of theoretically developed liquidus temperatures agree well with those obtained from the experimental work on ASTM F-75 alloy presented below.

3. Solidification modeling

The knowledge of phase diagram (solution of Eqs. (8)) makes possible to search for the solidification path using two extreme cases:

— lever rule (fully equilibrium conditions of the solidification process), or

— Scheil model [8].

Both of them assumes complete mixing in the liquid phase. The equilibrium solidification (lever rule), requires that diffusion in the solid be sufficiently fast to allow complete mixing in solid necessary to maintain equilibrium. The Scheil model assumes no diffusion in the solid. Therefore, such marginal behaviors are unlikely to occur in castings, and intermediate behavior is expected. Several other models were proposed up to date, letting for finite diffusion in liquid and solid phase [9], and finite diffusion in solid with complete mixing in liquid [10, 11]. In this paper the Scheil model has been used for preliminary calculations, as it gives more realistic results than the lever rule, for the systems exhibit solid phase diffusion coefficients much less than in liquid phase. The more sophisticated model, with back diffusion effects will be included in future work.

In the ternary system of the kind shown in Fig. 1, two stages should be considered: first, when the composition of liquid moves along smooth liquidus surface, and the second after the instant at which the solidification path reaches the minimum of eutectic valley (or valley floor). During the first stage single solid phase is formed, and the following Scheil model equations should be used:

$$(x_{L,i} - x_{S,i})\, df_S = (1 - f_S)\, dx_{L,i} \qquad (i = 1, 2). \tag{10}$$

When solidification path reaches the eutectic valley, solute balance equations can be expressed in the following form

$$x_{L,i}\, df_S - x_{S1,i}\, df_{S1} - x_{S2,i}\, df_{S2} = (1 - f_S)\, dx_{L,i} \qquad (i = 1, 2), \tag{11}$$

where

f_S — overall solid fraction, by the definition $f_S = V_S / V$, and

$$f_S = f_{S\alpha} + f_{S1} + f_{S2}, \tag{12}$$

$f_{S\alpha}$ — solid fraction attained just before entering eutectic valley, $f_{S\alpha} = V_{S,\alpha} / V$,

f_{S1}, f_{S2} — solid fractions of the phases (1 and 2) forming eutectic composition in the eutectic valley, by the definition $f_{S1} = V_{S1}/V$, $f_{S2} = V_{S2}/V$,
$x_{S1,i}$, $x_{S2,i}$ — mole fraction of component i in solid phases 1 and 2 respectively.
If the equation describing eutectic valley floor is known

$$x_{L,2} = \phi(x_{L,1}) \tag{13}$$

(it can easily be found from equilibrium phase diagram), the Scheil model can be expressed in more useful form

$$(1 - f_S)\, x_{L,i} = [(x_{L,i} - x_{S2,i}) - (x_{S2,i} - x_{S1,i})\,\beta]\, df_S \qquad (i = 1, 2), \tag{14}$$

where:
β — coefficient obtained by the elimination of f_{S1} and f_{S2} from the equations using eutectic valley floor function and differential mass balance ($df_S = df_{S1} + df_{S2}$)

$$\beta = -\frac{\dfrac{\partial \phi}{\partial x_1}\,(x_{L,1} - x_{S2,1}) - (x_{L,2} - x_{S2,2})}{\dfrac{\partial \phi}{\partial x_1}\,(x_{S2,1} - x_{S1,1}) - (x_{S2,2} - x_{S1,2})}. \tag{15}$$

An application of Scheil model in macro-micro solidification model is straightforward. Let us assume that enthalpy method is used for the macro heat transfer equation. At each time step m of length Δt^m, the enthalpy extracted from the control volume element is calculated from macro transport equation and is denoted ΔH^m. Then, splitting the solidification path into M small steps of equal length (for simplicity) $\Delta\tau = \Delta\tau^k = \Delta t^m/M$, we obtain $\Delta h = \Delta h^k = \Delta H^m/M$, and the micro scale energy balance of the control volume can be expressed as a function of differential increment of solid phase:

$$c_p (T^{k+1} - T^k) = \Delta h - L\Delta f_S^{k+1}. \tag{16}$$

Temperature T^{k+1} together with liquid composition $(x_{L,1},\ x_{L,2})^{k+1}$ must satisfy equilibrium conditions (8). Liquid composition should also follow Scheil model, which can be locally (where full differentials are substituted by finite increments) expressed in the form
— for the stage before entering eutectic valley,

$$x_{L,i}^{k+1} = x_{L,i}^k + \frac{1}{(1 - f_S^k)}\left[(x_{L,i}^k - x_{S,i}^k)\right] \Delta f_S^{k+1} \tag{17}$$

— and after entering eutectic valley

$$x_{L,i}^{k+1} = x_{L,i}^{k} + \frac{1}{(1 - f_S^k)} \left[\left[(x_{L,i}^{k} - x_{S2,i}^{k}) - (x_{S2,i}^{k} - x_{S1,i}^{k})\beta^k \right] \Delta f_S^{k+1} \right]. \qquad (18)$$

Introducing Scheil model relationships (17, 18) into equilibrium equations set (8) we can obtain an implicitly defined form for temperature as a function of solid fraction increment alone, $T^{k+1} = F(\Delta f_S^{k+1})$. Therefore, micro-scale energy balance (16) can be solved against solid fraction increment Δf_S^{k+1}, as the rest of variables are already known from the previous k step of the procedure. Special procedure will be required because of nonlinearity of the equation (16) due to an implicit definition of function $F(\Delta f_S^{k+1})$ (as a solution of nonlinear system of equations). Evaluation of solid fraction increments enable to determine composition of liquid phase (Eqs. (17, 18)) at new computational step $k + 1$, then the composition of solid phase(s) in equilibrium with liquid phase from equilibrium equation set (8) again. The procedure described here is continued until solid fraction reaches unity. If the assumption on complete mixing is not strictly satisfied, the simple modification of Scheil equation is possible. In such case, the left hand side of Eq. (10) should be multiplied by the constant ε, expressing the fraction of solute mixed into the bulk liquid [5].

Most practical metallurgical alloys solidify with a dendritic structure in a mold. The cobalt based alloys are not an exception from this rule. Both columnar and equiaxed dendrites can be formed in the ingot, depending on the local heat transfer conditions. Our attention will be focussed on equiaxed dendritic growth modeling, the experiment carried out for the ASTM F75 alloy has brouth results for this solidification regime. Obviously Scheil model described above has no ability to predict dendrites growth. From several literature models for the modeling of microstructure formation the model of Rappaz and coworkers [12] seems to be most reliable to be implemented in the multi-component system solidification. Original Rappaz model has been developed for binary alloys solidifying in equiaxed regime [13]. According to the classifiction introduced by Stefanescu [2], Rappaz model belongs to the deterministic simple geometry class models, which use dendrite tip kinetics model and solutal field to describe growth of equiaxed grain. It means that the solutal field is the main driving force of dendritic growth; thermal, curvature and capillary undercooling are neglected. The main simplifying assumptions of the model are:

— rapid thermal diffusion at the scale of the grain (uniform temperature equal to the dendrite tip temperature),
— the interdendritic liquid extends to the grain envelope remains in constant solute concentration (so called complete mixing of solute is achieved),
— the spherical diffusion envelope around the grain is replaced by the solute boundary layer of unknown thickness,
— an overall solute and thermal balance is satisfied at the scale of the grain.

As in Scheil model application, the micro scale energy balance of the control volume (16) is utilized. At every micro time step k of length $\Delta\tau$ the increment of solid phase Δf_S^{k+1} has to be predicted by the model.

Nucleation of the grain occurs in an undercooled melt, and can be described by the continuous model (Gauss normal distribution density function)

$$\frac{\partial n}{\partial(\Delta T)} = \frac{n_{\max}}{\Delta T_\sigma \sqrt{2\pi}} \exp\left[\frac{(\Delta T - \Delta T_n)^2}{2(\Delta T_\sigma)^2}\right]. \tag{19}$$

As soon as nucleus appears, it grows. At a given undercooling ΔT, the density of nuclei is given by the integral of the distribution function (19). Therefore, during consequent computational steps the number of active nuclei $n(t)$ is calculated, until the maximum undercooling (recalescence point) is reached.

In the control volume of constant value, the growth of active nuclei is described by the evolution of solid fraction with time t according to

$$f_S(t) = f_i(t) f_g(t) = f_i(t)\, n\,(t) \frac{4}{3} \pi R^3(t), \tag{20}$$

where internal solid fraction $f_i(t)$ is expressed as

$$f_i(t) = \Omega f(Pe(t)) \tag{21}$$

and correction function $f(Pe(t))$ [13]

$$f(Pe) = 1. + {}^1/_{\mathrm{Pe}} [1.5 + {}^1/_{\mathrm{Pe}} + 0.25\,({}^1/_{\mathrm{Pe}})^2]. \tag{22}$$

In the Eq. (21, 22) the grain Peclet number is used, based on the grain radius R, velocity of dendrite tip v and solute diffusion coefficient in liquid D.

The velocity of the dendrite tip is usually related to the undercooling by the classical power law

$$v = \eta \Delta T^2 \tag{23}$$

or can be evaluated via KGT (Kurz-Giovanola-Trivedi) model [14, 15].

The growth of the dendrite tips in a finite time interval $\Delta\tau$ advances the grain radius such that

$$\Delta R = v \Delta \tau. \tag{24}$$

The control volume energy balance equation (16) is used to calculate the temperature change $(T^{k+1} - T^k)$ during time step $\Delta\tau$, than other parameters describing solidification path can be evaluated for the current time step (namely $R(t)$, $f_g(t)$, $f_i(t)$, $f_S(t)$, $n(t)$ and liquid/solid concentrations of solute).

The dendrite tips velocity v is expected to be strongly influenced by solute segregation when the impingement of the grains takes place, and the solute boundary layers overlap. This phenomena is taken into account, verifying supersaturation according to the changes in bulk liquid concentration outside the grain, evaluated from the solute balance around the

grain boundaries. Also the geometrical considerations are to be incorporated, preserving overlapping of the grains at the final stage of building grains structure. Therefore the Johnson-Mehl or Avrami [16], Fraś [17], or Speich-Fisher [18, 19] procedure can be introduced. In present paper the modified Speich-Fisher impingement weighting function $\psi(f_g)$ for the grain fraction in Eq. (20) (this equation describes free grains growth) were used. The value of $\psi(f_g)$ is equal to unity before impingement, and

$$\psi(f_g) = \frac{f_g}{f_{g,\mathrm{imp}}} \left(\frac{1 - f_g}{1 - f_{g,\mathrm{imp}}} \right)^{1 - \frac{f_{g,\mathrm{imp}}}{f_g}} \tag{25}$$

after impingement, where $f_{g,\mathrm{imp}}$ is a value of grain fraction at the beginning of impingement (for equiaxed eutectic grains is equal to 0.72 (fcc) or 0.52 (bcc)).

When the dendritic grains are built, the interdendritic solute concentration equalizes with the solute concentration in the remnant liquid. Then the Scheil equations are adequate for the description of the solidification path.

The extention of the model described above for the multi-component alloy requires only an assumption that the kinetics of the dendrite growth is formally preserved, but the diffusion solutal fields are superimposed. Therefore total undercooling should be calculated according to the formula

$$\Delta T = \sum_i \Delta T_i, \tag{26}$$

if the KGT model for multi-component alloy (described below) [12], is to be used. When classical power law kinetics is used, the kinetic constant η should be fitted to the experimental data, using the same assumption and also the internal fraction should be related to the supersaturation of all constituents. Convex combination of individual supersaturiations produces the best results. The liquid phase concentrations together with solid phase ones (or instead of solid phase, partition coefficients k_i's) can be calculated using multi-component equilibrium equations (8). All other properties of the Rappaz at al. model are preserved.

The critical point for the model is to use reliable dendrites growth kinetics. For the ternary or multi-component alloys, dendrite growth model were proposed by Rappaz at al. [12] and Bobadilla et al. [20]. As in binary systems, the growth of dendrite is primarily assumed to be controlled by the solute diffusion. The mathematical solution of the diffusion problem for steady-state growing dendrite (described by the paraboloid of revolution) was derived by Ivantsov [21], who derived the relationship between supersaturation and the Peclet number associated with the moving tip of the dendrite tip paraboloid

$$\Omega = Iv\,(Pe), \tag{27}$$

where $Pe = r_p v/2D$, and Ivantsov function is defined by

$$Iv(z) = z\,E_1(z)e^z \tag{28}$$

$E_1(z)$ — an exponential integral function, $E_1(z) = \int_z^\infty [\exp(-u)/u]\,du$.

In the multicomponent system the diffusion fields around the dendrite tip associated with each constituent i can be expressed employing Ivantsov solution (27) with respect to the supersaturation and Peclet number of constituent i

$$\Omega_i = \frac{x^*_{L,i} - x_{O,i}}{x^*_{L,i} - x^*_{S,i}} = \frac{x^*_{L,i} - x_{O,i}}{x^*_{L,i}(1 - k_i)} = Iv(Pe_i). \tag{29}$$

By using linearized phase diagram approximation for multicomponent system, individual constituent undercooling reads

$$\Delta T_i = m_i x_{O,i}\left[1 - \frac{1}{1 - \Omega_i(1 - k_i)}\right] = m_i x_{O,i}\left[1 - \frac{1}{1 - Iv(Pe_i)(1 - k_i)}\right]. \tag{30}$$

Also, according to Rappaz model assumption, that the diffusion fields of all species can be superimposed, inserting Eq. (24) to Eq. (22), gives the relationship of the total undercooling of the dendrite tip to the supersaturations of all solute species.

Like in the binary system KGT model, the application of marginal stability criterion [22] leads to the approximate equation for the dendrite tip radius

$$r_p = 2\pi\left[\frac{\Gamma}{\sum_i m_i E_{xi}\,\zeta_x\,(Pe_i) - E}\right]^{1/2}, \tag{31}$$

where the solute gradient E_{xi} of constituent i near the tip, is given by

$$E_{xi} = -\frac{v}{D_i}\,x_{L,i}\,(1 - k_i).$$

For the low growth rates, average temperature gradient E can be neglected in Eq. (31), and the stability parameter $\zeta_x(Pe)$ approaches unity [15].

Combining Eq. (30) and linearized phase diagram relationship (neglecting curvature undercooling) in the form

$$T^* = T_L + \sum_i m_i\,(x_{L,i} - x_{O,i}), \tag{32}$$

where:

T^* — temperature at the dendrite tips,

we can derive the relationship between velocity of dendrite tips v (or tip radius r_p) as a function of total undercooling ΔT in the form of 2-nd order polynomial equation

$$A_1 (1/r_p)^2 + A_2 (1/r_p) + A_3 = 0\,, \tag{33}$$

where A_1, A_2, A_3 are the coefficients

$$A_1 = 4\pi\Gamma \qquad A_2 = \frac{2\sum m_i x_{O,i}(1-k_i)\,\zeta(Pe_i)}{1\ -\ (1-k_i)\,\Omega_i} \qquad A_3 = E\,.$$

The value of A_2 coefficient is implicity dependent on undercooling ΔT.

As pointed out by the authors of the procedure described above, the main difficulty becomes in the determination of the parameters related to the multi-component phase diagram (k_i's and m_i's). In our opinion, the direct substitution of binary counterparts, and linearization of multi-component phase diagram can lead to the erroneous results, which we acknowledged in the case of Co-Cr-Mo alloy.

The alternative solution, as described in [23], represents the TLSM procedure applied to the postulated multi-component alloy Rappaz type solidification model, in order to obtain estimates for the nucleation and growth kinetic parameters. Obtained fitting results differs from ones predicted by the KGT multi-component model. The KGT predictions and fitted kinetic model are shown in Fig. 2.

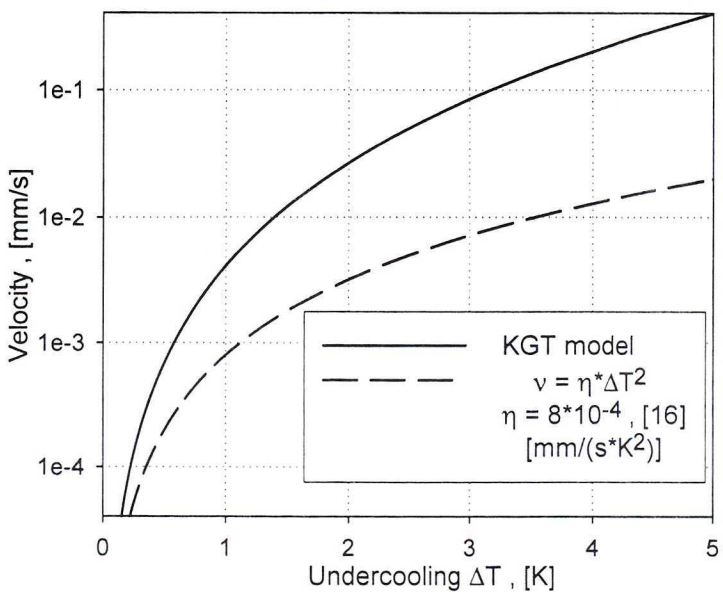

Fig. 2. Kinetic models of solidification, velocity of dendrite tip *vs* undercooling

4. Experimental investigations

The experimental studies were conducted using the computer-aided thermal analysis described thoroughly in the paper [24]. Three compositions of the alloy (ASTM F-75) were examined, with varying carbon content. The composition of the alloys are presented in the Table 2.

TABLE 2

Chemical composition of the selected alloys

Sample	Composition (wt. %)								
	C	Mn	Si	Ni	Cr	Mo	Fe	W	Co
1 and 2	0.09	0.06	0.05	0.05	26.52	6.18	0.28	0.04	balance
3 and 4	0.18	0.06	0.06	0.06	26.28	6.11	0.04	0.04	balance
5 and 6	0.27	0.07	0.066	0.068	27.26	6.67	0.57	0.04	balance

The alloys were melted under an inert atmosphere of argon in an electrical induction furnace equipped with a high alumina crucible. In each experiment the load consisted of 1000 gr of alloy. The molten metal was heated up to 1600°C. Alloy samples were poured into small alumina crucibles (3 cm of internal diameter and 4 cm of height) preheated to 1000°C, equipped with thermocouples type *B*. The alumina crucibles were cooled under different conditions to achieve different cooling rates. A detailed diagram of the experimental set up for the acquisition of the temperature-time data was presented in our paper [24]. For the acquisition and managing of the data the commercial program Workbench of Strawberry Co. was used, being registered the signals with a frequency of 1 Hz. Data were acquired and stored with accuracy of 0.1°C. For each set of experimental conditions, the experiment was repeated three times for assuring reproducibility.

The thermal investigations was complemented by the metallografic analysis and microanalysis. The solidified samples were sectioned transversely approximately 15 mm from the bottom of the sample. The samples were firstly polished and secondly etched with a specific chemical reactive (5 volumes of concentrated HCl and 1 volume of oxygenated water). The identification and quantification of the phases were made using an image analysis system, and the microanalysis was made using Energy Dispersive Spectrometry (EDS) and Scanning Electron Microscopy (SEM).

The cooling curves recorded for each sample were smoothed using Fourier series and their derivatives were calculated numerically point by point using the Savitzky-Golay algorithm [25]. Once the first derivative was obtained for each experiment, the corresponding zero curve was generated, employing commercial program Table Curve 2D of Jandel Scientific. Then, the latent heat of solidification was evaluated using procedure described in [24] and their values are given in Table 3.

TABLE 3

Latent heat of solidification

Sample	C (wt. %)	ΔH(KJ/Kg)	std. dev.
1 and 2	0.09	183,42	9.22
3 and 4	0.18	210.02	8.08
5 and 6	0.27	230.48	5.65

The microstructure and appearing phases were identified using an optical microscope. It was possible to observe the dendritic equiaxed structure of the grains, with inter- and intragranular carbides reach phases of the block morphology aligned in the interdendritic region.

In the Table 4 the cooling rates and corresponding grain sizes, measured using the planimetric method for each sample are presented. It can be observed that the grain size is a direct function of the cooling rate. No significant effect of the carbon content on grain size was observed.

TABLE 4

Cooling rates *vs* grain sizes and carbon content

Sample	C (wt. %)	Cooling Rate Q (°C/s)	Grain Size (nominal diameter, mm)
1	0.09	7.90	4.5
2	0.09	5.25	5.4
3	0.18	9.06	4.3
4	0.18	6.90	5.2
5	0.27	12.55	3.9
6	0.27	7.07	4.5

In order to characterize the segregation of main alloying elements (Cr and Mo) a linear analysis across the dendritic and inter-dendritic regions by scanning microscope was made. Fig. 3. shows an example of such an analysis.

The regions analyzed were selected to assure that the line analysis covers three secondary dendrite arms and their adjacent interdendritic regions (white line in the figure). The scanning electron microscope signal proportional to the Co, Cr, Mo, C along the line are also shown in Fig. 3. The partition coefficient values of constituent i were calculated according to the formula

$$k_i = \frac{x_{1,i}}{x_{2,i}}, \tag{34}$$

where:

$x_{1,i}$, $x_{2,i}$ — concentrations of constituent i in phase 1 and 2, respectively.

The values of measured partition coefficients are presented in Table 5 for all samples. The results show that the partition coefficients are more sensitive on cooling rate than on carbon content.

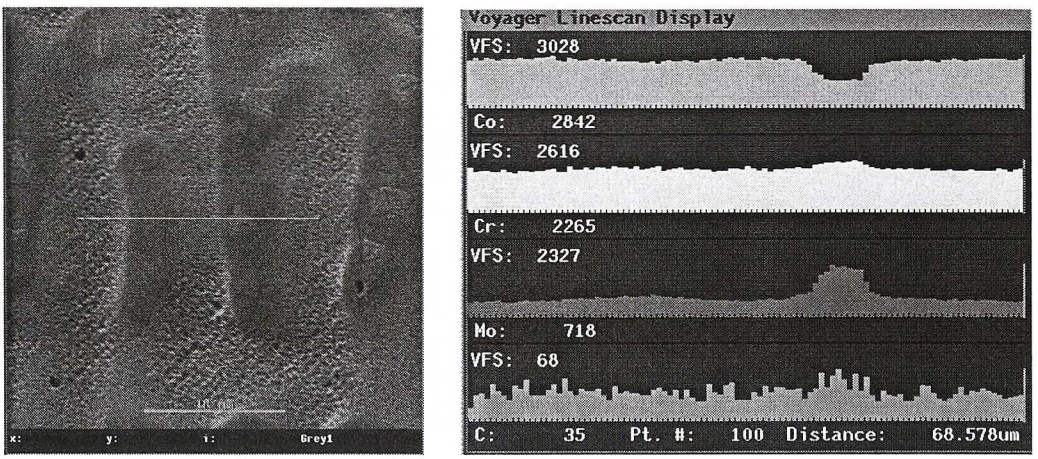

Fig. 3. Line analysis using SEM

TABLE 5

Partition coefficient values for Cr and Mo as a function of carbon content and cooling rate (dendritic region/interdendritic region)

Sample	C (wt. %)	Cooling Rate Q (°C/s)	k_{Cr}	std. dev.	k_{Mo}	std. dev.
1	0.09	7.90	0.863	0.011	0.684	0.047
2	0.09	5.25	0.850	0.016	0.615	0.017
3	0.18	9.06	0.892	0.008	0.697	0.030
4	0.18	6.90	0.858	0.025	0.653	0.043
5	0.27	12.55	0.898	0.005	0.742	0.002
6	0.27	7.07	0.887	0.029	0.687	0.024

5. Numerical results

The computer program utilizing the multi-component Rappaz model and multi-component Scheil model discussed in previous sections was developed to study solidification path of Co-Cr-Mo alloys. In order to simplify calculations, it is useful to carry out thermodynamic computations first.

It is also useful to approximate representation of the liquidus surface (polynomial approximation of the several data obtained from the solution of equilibrium equations (8)), eutectic valley floor equation (13), composition of solid phases in equilibrium with composition of eutectic valley floor liquid (in the form parameterized by the composition of liquid to enable simple evaluation of corresponding composition of solid in equilibrium with liquid — equilibrium chord). The results of our calculations are presented in Appendix 1.

The form of the computer program is that it can be used for interpreting measurement results and can be incorporated in the standard macro enthalpy code, to be used for practical engineering purposes. The data required, behind all parameters characterizing alloy thermo-physical properties and equilibrium diagram, consist of heat rejected from the

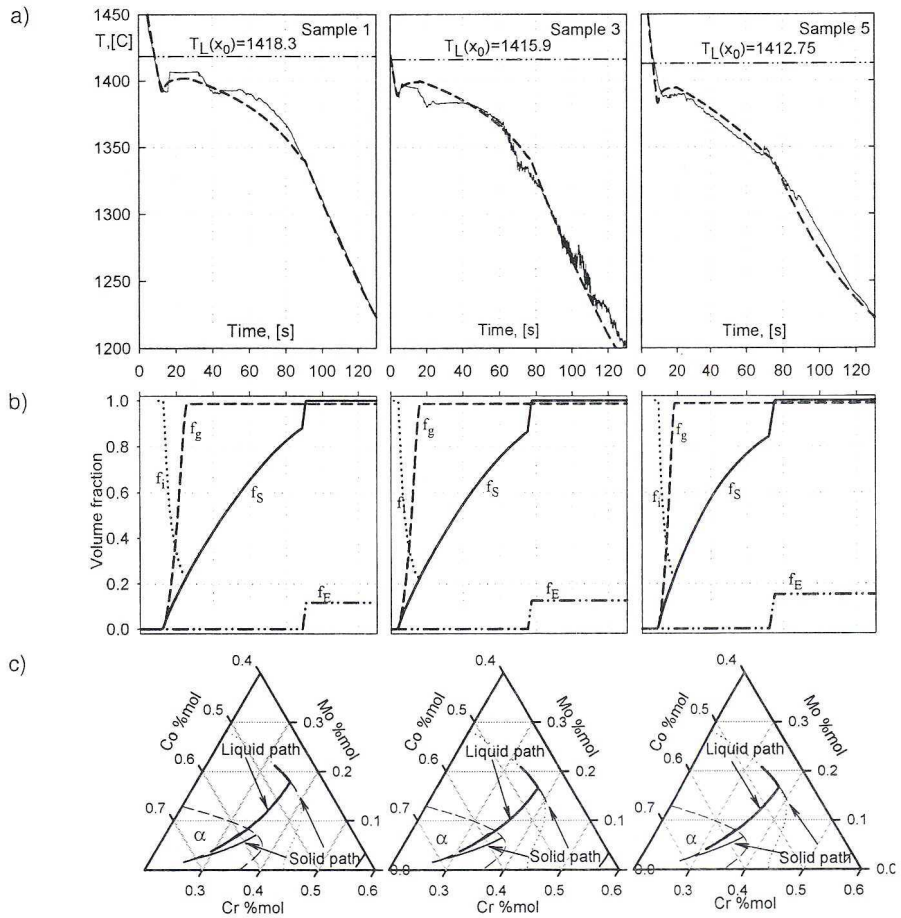

Fig. 4. Model predictions for three samples: a) cooling curves (solid lines) *vs* model predictions (dashed lines), $T_L(x_0)$ — liquidus temperature for the initial alloy composition; b) volume fractions evolution, f_S — solid fraction, f_g — grain fraction, f_i — internal solid fraction of the grain, f_E — eutectic valley phase; c) solidification paths in ternary system Co-Cr-Mo

control volume, macro time step, composition of the alloy, and parameters characterizing the stage of the chilling process (i.e. initial solid fraction, etc.).

The cooling curves for 3 samples and corresponding model predictions for the time evolution of temperature, fraction of phases, and corresponding solidification paths are presented in Fig. 4.

The calculated and measured final grain sizes for all samples are given in Table 6.

TABLE 6

Measured and predicted grain sizes

Sample	Cooling Rate Q (°C/s)	Measured grain size (mm)	Predicted grain size (mm)	Predicted fraction of eut. valley phase, %
1	7.90	4.5	4.56	11.86
2	5.25	5.4	5.23	11.80
3	9.06	4.3	4.33	13.38
4	6.90	5.2	4.81	13.27
5	12.55	3.9	4.08	15.70
6	7.07	4.5	4.76	15.35

Partition coefficients, which could be compared with measured values, have been calculated using appropriate averaging procedure: the concentration of solute constituents in dendrite arms were averaged against solid volume attained at grains growth end as an integral average. The same procedure has been used for interdendritic phase and eutectic valley phase separately. The results are compared with measured coefficient values in Table 7.

TABLE 7

Measured partition coefficients *vs* predicted for the dendritic/interdendritic phase

Sample	Cooling Rate Q (°C/s)	k_{Cr} measured	std. dev.	k_{Cr} predicted	k_{Mo} measured	std. dev.	k_{Mo} predicted
1	7.90	0.863	0.011	0.910	0.684	0.047	0.694
2	5.25	0.850	0.016	0.909	0.615	0.017	0.682
3	9.06	0.892	0.008	0.915	0.697	0.030	0.711
4	6.90	0.858	0.025	0.910	0.653	0.043	0.698
5	12.55	0.898	0.005	0.917	0.742	0.002	0.739
6	7.07	0.887	0.029	0.915	0.687	0.024	0.705

Unfortunately, lack of the more precise data concerning carbides formation, precluded us to incorporate exact analysis on their formation during solidification process. Therefore,

only redistribution of the carbon is traced, using constant value coal partition coefficient. It is believed, that constant enrichment of the liquid phase with carbon, at the final stage of solidification forms the conditions favoring formation of carbides in the interdendritic region and finally in the intergranular remnant liquid. In this way, the early formation of carbides (in interdendritic region) will be promoted by the high cooling rate by means of deeper segregation process and lower temperature.

6. Conclusions

The extended Rappaz model with classical power law dendrite tips kinetics enables prediction of microstructure formation in ASTM F-75 alloy. Thermodynamic representation of equilibrium ternary system Co-Cr-Mo, together with Scheil model for multicomponent system applied in solidification modeling just after formation of the dendritic grain structure allow to predict full solidification path. The model results have been verified using cooling curve analysis and metallografic investigations. It seems, that the model can be used in engineering applications for solidification simulations. Both, experimental and numerical results showed that: the grain structure is mainly influenced by the cooling rate, the partition coefficients exhibit significant dependency on the cooling rate (especially for molybdenum), the high cooling rate promotes early formation of fine intragranular carbides. The experimentally obtained values of latent heat of solidification exhibit important dependency on the initial carbon content, and cannot be ignored in solidification simulations. Further experimental investigations should be oriented on the nucleation and growth kinetics of carbides. It would result in complete description of the solidification modeling of cobalt based alloys of ASTM F-75 type.

Acknowledgments

Authors are grateful for CONACYT (Grant No. 31340-U) and KBN (Grant No. 11.11.180.136) for financial support during this study.

Appendix 1

The equation defining eutectic valley floor compositions (Eq. (13)):

$$x_{Cr,ev}(x_{Mo}) = 0.4404 - 0.6065x_{Mo} + 11.3966(x_{Mo})^2 - 98.9365(x_{Mo})^3 + 278.6819(x_{Mo})^4 - 290.7031(x_{Mo})^5.$$

The equation defining temperature along eutectic valley floor (parametrized consistently with eutectic valley composition equation):

$$T_{ev}(x_{Mo}) = 1668.0 - 406.646x_{Mo} + 84.767(x_{Mo})^2 + 1857.600(x_{Mo})^3 + 14273.078(x_{Mo})^4 - 45226.909(x_{Mo})^5 \text{ [K]}.$$

The equations defining composition of solid phase S_1 (reach with Co) in equilibrium with liquid of composition defined by the $(x_{Cr}, x_{Mo})_{ev}$ on eutectic valley:

$$x_{Mo,S1}(x_{Mo}) = 0.0 + 0.4424x_{Mo} - 0.6884(x_{Mo})^2 + 2.4378(x_{Mo})^3$$

$$x_{Cr,S1}(x_{Mo,S1}) = 0.3635 + 0.5753x_{Mo,S1} + 6.6946(x_{Mo,S1})^2 - 299.020(x_{Mo,S1})^3 + 1058.189(x_{Mo,S1})^4.$$

The equations defining composition of solid phase S_2 (reach with Cr) in equilibrium with liquid of composition defined by the (x_{Cr}, x_{Mo}) on eutectic valley:

$$x_{Mo,S2}(x_{Mo}) = 0.0 + 2.0931x_{Mo} - 44.2787(x_{Mo})^2 + 392.7295(x_{Mo})^3 - 1085.4963(x_{Mo})^4 + 955.0428(x_{Mo})^5.$$

$$x_{Cr,S2}(x_{Mo,S2}) = 0.5609 + 0.3785x_{Mo,S2} - 7.7993(x_{Mo,S2})^2 + 22.9800(x_{Mo,S2})^3 - 28.7430(x_{Mo,S2})^4 + 12.7715(x_{Mo,S2})^5.$$

The polynomial approximation of liquidus surface close to the Co vertex in the Gibbs triangle:

$$T_L(x, y) = 1765.134 - 19.342x - 694.700y - 902.500x^2 + 928.797xy + 665.511y^2 + 1369.038x^3 - 1001.603x^2y - 916.515xy^2 - 347.550y^3 - 831.766x^4 + 299.860x^3y + 169.649x^2y^2 - 5.873xy^3 - 138.337y^4,$$

where:

x — x_{Cr}, molar concentration of chromium, $x \in [0,1]$,

y — x_{Mo}, molar concentration of molybdenum, $y \in [0,1]$,

x, y must obey inequality $x - x_{Cr,ev}(y) = x_{Cr} - x_{Cr,ev}(x_{Mo}) \leq 0$

T — liquidus temperature for the composition (x_{Cr}, x_{Mo}), [K].

REFERENCES

[1] J. Marciniak, Biomaterials, Wyd. Pol. Śląskiej, Gliwice 2002 (in Polish)

[2] D.M. Stefanescu, Methodologies for and Performance of Macro Transport- Transformation Kinetics Modeling of Cast Iron, J. Adv. Materials Research **4–5**, 89–104 (1997).

[3] M. Rettenmayr, Computational Methods in Materials Science, MRS. Symp. Proc., **278**, 325–330 Ed. J. E. Mark et al., (Pittsburgh, PA: MRS. 1992).

[4] D.A. Porter, K.E. Easterling, Phase Transformations in Metals and Alloys, Van Nostrand Reinhold Co. (UK), 1994.

[5] S. Chen, W. Oldfield, Y.A. Chang, M.K. Thomas, Modelling Solidification of Turbine Blades Using Theoretical Phase Relationships, Met. Trans. **25A**, 1525–1533 (1994).

[6] K.C. Chou, Y.A. Chang, Ber. Bunsenges. Phys. Chem. **93**, 735–41 (1989).
[7] I.G. Eroschenkova, A.M. Zaharov, B.G. Olenicheva, Metalurgical Alloys Phase Diagrams, 60–62 Moskva (1985).
[8] E. Scheil, Z. Metallk. **34**, 70 (1942).
[9] L. Nastac, D.M. Stefanescu, An Analytical Model for Solute Redistribution during Solidification of Planar, Columnar, or Equiaxed Morphology, Met. Trans. **24A**, 2107–2118 Sept. (1993).
[10] H.D. Brody, M.C. Flemings, Trans TMS-AIME **236,** 615 (1966).
[11] W. Wołczyński, Modelling of Transport Phenomena in Crystal Growth, Ed. by J.S. Szmyd and K. Suzuki, WIT Press, 1119–59 Sothampton-Boston (2000).
[12] M. Rappaz, S.A. David, J.M. Vitek, L.A. Boatner, Analysis of Solidification Microstructures in Fe-Ni-Cr Single Crystals Welds, Met. Trans. **21A**, 1767–82 June (1990).
[13] Ph. Thevoz, J.L. Desbiolles, M. Rappaz, Modeling of Equiaxed Microstructure Formation in Casting, Met. Trans. **20A**, 311–22 (Feb. 1989).
[14] W. Kurz, B. Giovanola, R. Trivedi, Theory of Microstructural Development during Rapid Solidification, Acta Metall. **34**, 5, 823–30 (1986).
[15] J. Lipton, W. Kurz, R. Trivedi, Rapid Dendrite Growth in Undercooled Alloys, Acta Metall. **35**, 4, 957–64 (1987).
[16] M. Rappaz, International Materials Reviews **34(3)**, 93–123 (1989).
[17] E. Fraś, Crystallization of Metals and Alloys, PWN, Warsaw, 1992 (in Polish).
[18] G.R. Speich, R.M. Fisher, Recrystallization, Grain Growth and Textures, ASM, Metals Park, 563–98 OH, (1996).
[19] J. Ni, R.J. Feller, C. Beckermann, Modelling of Casting, Welding, and Advanced Solidification Processes-V, M. Rappaz, M. Ozgu, K.W. Mahin, Eds., TMS, 675–82, Switzerland, 1990.
[20] M. Bobadilla, J. Lacaze, G. Lesoult, Influence des conditions de solidification sur déroulement de la solidification des aciers inoxydables austenitiques, J. Cryst. Growth. **89**, 531–544 (1988).
[21] G.P. Ivantsov, Thermal and Diffusion Processes in Crystal Growth, Dokl. Akad. Nauk SSSR **58**, 567 (1947).
[22] W.W. Mullins, R.F. Sekerka, J. Appl. Phys. **35**, 444 (1964).
[23] Z. Kolenda, J. Donizak, J.C. Escobedo Bocardo, Least Squares Adjustment of Mathematical Model of Heat and Mass Transfer Process during Solidification of Binary Alloys, Met. Trans. **30B**, 505–513 June 1999.
[24] J.C. Escobedo Bocardo, M.A. Ramirez, Z. Kolenda, J. Donizak, Computer Aided Cooling Curve Analysis Applied to a Co-Cr-Mo System, Archives of Metallurgy **45(2)**, 185–196 (2000).
[25] A. Savitzky, M. Golay, Smoothing and Differentiation of Data by Simplified Least Squares Procedures, Anal. Chem **36**, 8, 309–313 (1964).

REVIEWED BY: WALDEMAR WOŁCZYŃSKI
Received: 20 December 2002.